Ionic displacement correlations from the zero-point motion of pressurized solid argon

Hadley M. Lawler
Department of Physics, University of Maryland, College Park, Maryland 20742-4111, USA

Eric K. Chang
INFM National Center on nanoStructures and bioSystems at Surfaces and Dipartimento di Fisica, Università di Modena e Reggio Emilia, Via Campi 213/A, 41100 Modena, Italy

Eric L. Shirley
Optical Technology Division, National Institute of Standards and Technology, 100 Bureau Drive, Stop 8441, Gaithersburg, Maryland 20899-8441, USA

(Received 26 September 2003; revised manuscript received 20 January 2004; published 11 May 2004)

We have performed first-principles calculations of the elastic constants and phonon dispersion for solid argon at pressures ranging from 3.1 GPa to 70 GPa. We also report our calculation of the spatial correlation function for the ground state and its pressure dependence. Arbitrary Cartesian displacements and lattice-site separations are considered. Analytical results, which rely only on knowledge of the elastic constants, are compared with results based on the calculated phonon dispersion throughout the Brillouin zone, and agree satisfactorily. The correlations are presented for pressures ranging from 3.1 GPa to 70 GPa, and the results suggest that the anharmonic character of the crystal's ground state is more significant at low pressure.

DOI: 10.1103/PhysRevB.69.174104 PACS number(s): 62.50.+p, 63.20.Dj, 62.65.+k

I. INTRODUCTION

Equal-time, ion-ion correlation functions have been of theoretical interest since the early days of theoretical lattice dynamics.[1,2] The autocorrelations appear in the Debye-Waller factor and crystal melting criteria,[3,4] and the two-site correlations are related to a variety of measurable effects. They have been shown to imprint ''extra spots'' on the diffuse, elastic x-ray scattering background arising from thermal fluctuations,[5,6] and more recently, experiments concerning their relevance to extended x-ray-absorption fine structure[7] and electronic motion[8] have been performed. Bond-charge models have been used to calculate a few of the correlations in covalent semiconductors.[9]

Perhaps of particular theoretical interest, the correlation functions are relevant to lattice dynamics beyond the harmonic approximation. A body of theoretical work over the last five years marks a breakthrough in the first-principles considerations of anharmonic effects,[10–13] and the correlation functions can be applied to the calculation of related matrix elements. As an illustration of this, a term in the potential energy which is cubic in ionic displacements hybridizes the crystal's ground state with a state in which a mode is occupied by a single phonon. The corresponding matrix element can be expressed as a phased sum of fourth-order correlations multiplied by appropriate anharmonic potential coefficients. These fourth-order correlations can be contracted into products of pairwise correlations over the ground state, which we evaluate here. In a related connection between anharmonic perturbation theory and the correlation functions, Van Hove has posited the ratio of the autocorrelation length to ion separation as the expansion parameter with which to rank the multiphonon processes.[14]

Commonly, the zero-point ionic motion's greatest experimental significance is in the study of the lightest elements, and would not be prominent in a system such as argon. However, at zero temperature, nonzero values of the correlation functions can generally be attributed solely to the quantum-mechanical zero-point motion of the ground state.

We have calculated the ground-state correlations in solid argon, for arbitrary lattice-site separation, using (1) current first-principles methods and (2) analytic expressions from long-known approximations to the phonon spectrum.[2] Argon is a convenient choice for the calculation of these correlations. It is an insulating crystal with a single atom in the unit cell, and so complications associated with optical phonons and a Fermi surface need not be addressed. A comparison of results obtained via the two approaches is interesting as a mutual check on the modern technique, where the results are highly numeric in nature, and the more traditional analytic methods, which are computationally transparent but rely on more approximate assumptions.

II. PRESSURIZED SOLID ARGON

Advanced spectroscopic techniques probing materials at high pressure have recently allowed detailed experimental investigation of structural properties of solid argon,[15–18] which is of interest as a fundamental solid. The equation of state, and the pressure dependence of elastic constants and phonon dispersion have been reported. These investigations and accompanying pair potential calculations have been complimented by first-principles studies which rely on density-functional theory.[19–23] There is general agreement between the theoretical and experimental results, and the degree of correspondence increases at higher pressures. This may be expected, since density-functional theory accounts for electronic correlations only when there is charge-density overlap, and hence cannot model strict van der Waals effects,[19] and at lower densities, or lower pressures, the relative importance of the van der Waals forces obviously grows.

Nevertheless, the theoretically obtained properties are rea-

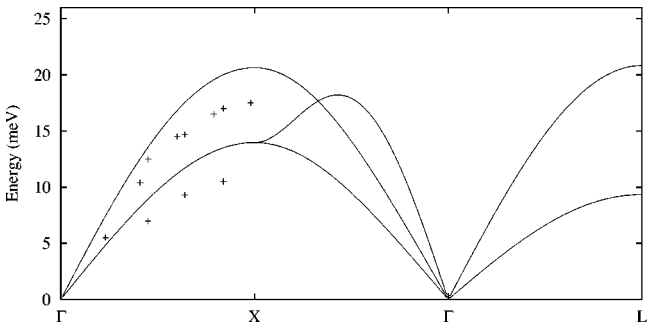

FIG. 1. Calculated phonon dispersion of argon at 3.1 GPa for a few high-symmetry lines, and experimental data from Ref 15.

sonable even to nearly ambient pressure when the generalized-gradient functional is employed. The local-density approximation,[24] with which the present results are calculated, has been shown to give an equation of state of poorer agreement with measurement than the generalized-gradient approximation.[20] Indeed, at lower pressures, the associated densities we report are 10% to 15% higher than those obtained from experiment. In addition to the local-density approximation, our calculations are performed with pseudopotentials and a plane-wave basis.[25–27] All values we report were checked for convergence with respect to Brillouin-zone sampling and plane-wave cutoff.

The pressures we report are evaluated by first calculating points along a total energy vs volume curve, and then obtaining a best fit to the Murnaghan equation of state. At 3.1 and 6.7 GPa, the values are checked by introducing an internal strain. When the solid is pressurized, the energy density E is modified from its equilibrium value, E_0, by a linear as well as quadratic term with the uniaxial strain parameter e_{11}, $E=E_0-Pe_{11}+\frac{1}{2}c_{11}e_{11}^2$. The coefficient in the quadratic term is the standardly defined elastic constant. The linear term represents work done as the volume varies with the strain, and the coefficient P represents the pressure. The pressures obtained from the strain calculation and from the equation of state agree to within 10%.

III. PHONON DISPERSION AND ELASTIC CONSTANTS

The phonon dispersion is calculated through a diagonalization of the dynamical matrix, which is calculated with lowest-order Hellmann-Feynman forces[28] and density-functional theory using wave-commensurate supercells. In this work we do not sample the anharmonic contributions to the forces, a task which, in principle, is also manageable. Figure 1 displays theoretical phonon dispersion along a few high-symmetry lines for a crystal at 3.1 GPa, and how it compares to experimental dispersion along the (100) direction at the same pressure. The uncertainty in the experimental data points is less than ± 1 meV. Our result and the discrepancy from experiment is quite similar to that of other recent local-density approximation work.[20] Our corresponding theoretical density is 2.7 g/cm^3. At 6.7 GPa, or a density of 3.0 g/cm^3, the frequency of the longitudinal mode at the Brillouin-zone boundary along (100) increases to 26 meV from the value 21 meV at 3.1 GPa. At 10 GPa and 70 GPa, the value is, respectively, 29 meV and 53 meV, and the corresponding densities are 3.2 g/cm^3 and 4.6 g/cm^3.

The elastic constants are reported through evaluation of the low-momentum speeds of sound from the calculated dispersion relations. At 6.7 GPa, the constants are computed twice, the second method entails monitoring of the total energy over a range of internal strains. The two values are identical to the numerical accuracy reported for c_{11}, and differ by about 20% for c_{12} and c_{44} (for c_{12} the strain-derived value is lower and for c_{44} the strain-derived value is higher). The calculated elastic constants for various crystal pressures are $c_{11}=36$ GPa, $c_{12}=24$ GPa, and $c_{44}=16$ GPa at 3.1 GPa; $c_{11}=54$ GPa, $c_{12}=38$ GPa, and $c_{44}=23$ GPa at 6.7 GPa; $c_{11}=72$ GPa, $c_{12}=50$ GPa, and $c_{44}=33$ GPa at 10 GPa; and $c_{11}=270$ GPa, $c_{12}=200$ GPa, and $c_{44}=130$ GPa at 70 GPa. Our values for the elastic constants differ from those of some earlier studies by more than 50% at 3.1 GPa. The agreement improves at higher pressures to about 10% at 70 GPa.

IV. EXACT FORMULAS FOR THE CORRELATION FUNCTION

The displacement of an ion at lattice site **R** along Cartesian direction i is written as the sum over phonon creation and annihilation operators, indexed by wave vector and branch:

$$x_{i\mathbf{R}}=\frac{1}{\sqrt{N}}\sum_{\mathbf{k}\nu} e^{i\mathbf{k}\cdot\mathbf{R}}\sqrt{\frac{\hbar}{2m\omega_{\mathbf{k}\nu}}}(a_{\mathbf{k}\nu}+a^{\dagger}_{-\mathbf{k}\nu})u_{\mathbf{k}\nu i}\,, \qquad (1)$$

where the right-hand side makes reference to phonon polarization, and to square roots of the ionic mass, phonon frequency, and number of lattice sites (or independent wave vectors) in the denominators.

The ground-state expectation value of the product of two such operators, defined to be the ground-state ion-ion correlation, is

$$\langle x_{i\mathbf{R}+\mathbf{S}}x_{j\mathbf{R}}\rangle=\frac{1}{N}\sum_{\mathbf{k}\nu} e^{i\mathbf{k}\cdot\mathbf{S}}\frac{\hbar}{2m\omega_{\mathbf{k}\nu}}u_{\mathbf{k}\nu i}u^{*}_{\mathbf{k}\nu j}\,, \qquad (2)$$

because only terms first creating and then annihilating the same phonon are nonzero, and because of the relation, $u_{-\mathbf{k}\nu}=u^{*}_{\mathbf{k}\nu}$. The vectors $\{\mathbf{u}_{\mathbf{k}\nu}\}$ form an orthonormal, diagonal basis for the dynamical matrix $\mathbf{D}(\mathbf{k})$, and its eigenvalues are the squares of the phonon frequencies, implying the relations

$$\sum_{\nu}\frac{u_{\mathbf{k}\nu i}u^{*}_{\mathbf{k}\nu j}}{\omega_{\mathbf{k}\nu}}=[D^{-1/2}(\mathbf{k})]_{ij}$$

and

$$\langle x_{i\mathbf{R}+\mathbf{S}}x_{j\mathbf{R}}\rangle=\frac{\hbar}{2mN}\sum_{\mathbf{k}} e^{i\mathbf{k}\cdot\mathbf{S}}[D^{-1/2}(\mathbf{k})]_{ij}\,. \qquad (3)$$

The result is that the dynamical matrix contains all the information necessary to calculate the ion-ion correlation functions.

V. APPROXIMATE FORMULAS

A cautious analysis of the correlations benefits from an analytic check on the numeric results derived from the above expressions. The primary concern with the numerical results is the singularity which occurs in Eq. (3) as **k** tends to zero. Further, the coherent nature of the contributions to the correlations from small-momentum wave vectors may indicate sensitivity to the sampling about the Γ point. For these reasons as well as for the sake of comparing exact and heavily computational results with common approximations in handling the phonon spectrum, such as the Debye model, we perform a systematic analysis of the correspondence between the two. The comparison also provides a measure of anisotropy's effect on the correlations.

Three approximations bridge the transition from the expression in Eq. (3) to an analytically treatable case. Two of the approximations are well known from the Debye model: taking the acoustic, small-momentum linear dispersion as valid throughout the whole Brillouin zone, and approximating the Brillouin zone itself as a sphere of the same volume. The other approximation forces an isotropic condition on the elastic constants.

The linear-dispersion approximation can be expressed through examination of the small-momentum expansion of the dynamical matrix. If we consider the Cartesian components of a deformation field $u_i(\mathbf{R})$ within the crystal, and the deformations vary slowly, the local energy density of a cubic system can be written[29] as

$$U=\frac{1}{2}c_{11}\sum_i\left(\frac{\partial u_i}{\partial R_i}\right)^2+\frac{1}{2}c_{44}\sum_i\sum_{j<i}\left(\frac{\partial u_i}{\partial R_j}+\frac{\partial u_j}{\partial R_i}\right)^2 + c_{12}\sum_i\sum_{j<i}\frac{\partial u_i}{\partial R_i}\frac{\partial u_j}{\partial R_j}, \tag{4}$$

where c_{11}, c_{12}, and c_{44} are the elastic constants.

Slowly varying deformations can be treated with a continuum model, where the Fourier transform of the strain field is defined as

$$u_i(\mathbf{k})=\frac{1}{\Omega_0}\int d^3\mathbf{r}u_i(\mathbf{r})e^{-i\mathbf{k}\cdot\mathbf{r}}, \tag{5}$$

and Ω_0 is the crystal volume. The dynamical matrix is

$$D_{ij}(\mathbf{k})=\frac{1}{\rho}\frac{\partial^2 U}{\partial u_i(-\mathbf{k})\partial u_j(\mathbf{k})}, \tag{6}$$

where ρ is the mass density, and the eigenvalues of the dynamical matrix are the squares of the phonon frequencies. Working out the equations of motion from Eq. (4), the small-momentum dynamical matrix for acoustic phonons is

$$\mathbf{D}(\mathbf{k})=\frac{1}{\rho}\begin{pmatrix} c_{11}k_x^2+c_{44}(k_y^2+k_z^2) & (c_{12}+c_{44})k_xk_y & (c_{12}+c_{44})k_xk_z \\ (c_{12}+c_{44})k_xk_y & c_{11}k_y^2+c_{44}(k_x^2+k_z^2) & (c_{12}+c_{44})k_yk_z \\ (c_{12}+c_{44})k_xk_z & (c_{12}+c_{44})k_yk_z & c_{11}k_z^2+c_{44}(k_x^2+k_y^2)\end{pmatrix}. \tag{7}$$

The second approximation is that of an isotropic crystal:

$$c_{11}=c_{12}+2c_{44}. \tag{8}$$

This condition reduces Eq. (7) to projections onto longitudinal and transverse modes:

$$\mathbf{D}(\mathbf{k})=\frac{c_{11}k^2}{\rho}|\hat{\mathbf{k}}\rangle\langle\hat{\mathbf{k}}|+\frac{c_{44}k^2}{\rho}(1-|\hat{\mathbf{k}}\rangle\langle\hat{\mathbf{k}}|), \tag{9}$$

and makes the speed of sound independent of wave vector.

The third, Debye-like approximation defines a sphere of radius k_{DB} and replaces the Brillouin-zone integration with integration over the sphere volume, implying

$$\frac{4\pi}{3}k_{DB}^3=\Omega_{BZ}. \tag{10}$$

VI. ANALYTICAL AND NUMERICAL RESULTS AT 6.7 GPa

Via the three approximations above, we can make a stepwise transition from realistic argon to a model system with analytical expression of the correlation function. As each successive approximation is made, we monitor its effect on the correlation function by making a numerical calculation, and then perform the algebraic computation for the analytically treatable approximations. Numerical calculations are done for the following cases: (1) exact realistic calculation, (2) legitimacy of the small-momentum phonon spectrum, Eq. (7), and (3) Eq. (7) and isotropy with regard to lattice properties, Eq. (8). The isotropic elastic constants are selected to meet Eq. (8) and so as to not affect their average value or that of the bulk modulus, giving $c_{11}=69$ GPa, $c_{12}=33$ GPa, and $c_{44}=18$ GPa.

When the substitution of a sphere for the actual Brillouin zone is joined with the conditions, Eqs. (7) and (8), Eq. (3) becomes

$$\langle x_{i\mathbf{R}+\mathbf{S}}x_{j\mathbf{R}}\rangle=\frac{\hbar}{2m\Omega_{BZ}}\int d^3\mathbf{k}e^{i\mathbf{k}\cdot\mathbf{S}}\sqrt{\frac{\rho}{k^3}}\left(\frac{k_ik_j}{\sqrt{c_{11}}}+\frac{k^2\delta_{ij}-k_ik_j}{\sqrt{c_{44}}}\right). \tag{11}$$

The integration is performed over the sphere of Eq. (10). Making the following definitions:

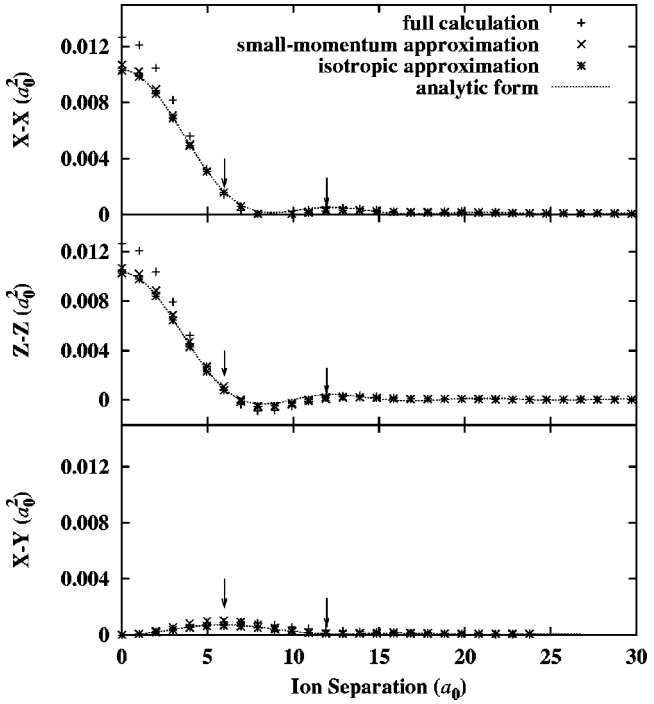

FIG. 2. Independent displacement-displacement correlations along the lattice-separation direction (110) at 6.7 GPa. Plots are for correlations in which both ions are displaced along the *x* direction (top), for both ions displaced along the *z* direction (middle), and for one ion displaced along the *x* direction and the other along the *y* direction (bottom). Correlations for orientations not shown are zero by symmetry or symmetry equivalent to those shown. The nearest sites are represented by arrows. The crosses represent the full calculation and the dashed line represents the analytical result. The intermediate approximations are represented by the diagonal crosses (small-momentum approximation) and by the stars (small-momentum approximation and isotropic approximation).

$$\phi = k_{DB} S,$$

$$\alpha_i = 1 - \left(\frac{S_i}{S}\right)^2,$$

$$\gamma_{ij} = \frac{S_i S_j}{S^2},$$

$$\frac{1}{c} = \sqrt{\rho}\left(\frac{1}{\sqrt{c_{11}}} - \frac{1}{\sqrt{c_{44}}}\right),$$

and performing the integration, the result for $i=j$ is

$$\langle x_{i\mathbf{R}+\mathbf{S}} x_{i\mathbf{R}}\rangle = \frac{\hbar}{2m\Omega_{BZ}} \frac{4\pi}{S^2}\left\{ \sqrt{\frac{\rho}{c_{44}}}(1-\cos\phi) + \frac{1}{c}\left[2\alpha_i - 1 + (\alpha_i - 1)\cos\phi + (2-3\alpha_i)\frac{\sin\phi}{\phi}\right]\right\}, \quad (12)$$

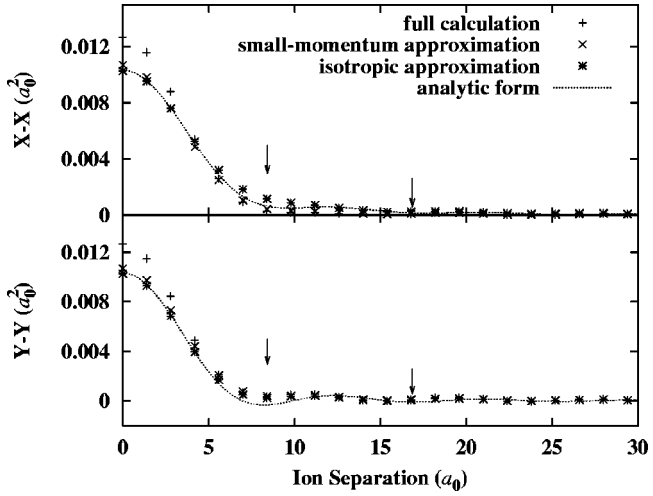

FIG. 3. Independent, nonzero displacement-displacement correlations along the lattice-separation direction (200) at 6.7 GPa. Plots are for correlations in which both ions are displaced along the *x* direction (top), and for both ions displaced along the *y* direction (bottom). Correlations for orientations not shown are zero by symmetry or symmetry equivalent to those shown. The nearest sites are represented by arrows. The crosses represent the full calculation and the dashed line represents the analytical result. The intermediate approximations are represented by the diagonal crosses (small-momentum approximation) and by the stars (small-momentum approximation and isotropic approximation).

and for $i \neq j$ the result is

$$\langle x_{i\mathbf{R}+\mathbf{S}} x_{j\mathbf{R}}\rangle = \frac{\hbar}{2m\Omega_{BZ}} \frac{4\pi}{S^2}\gamma_{ij}\left(\frac{3\sin\phi}{\phi} - \cos\phi - 2\right). \quad (13)$$

Figures 2 and 3 represent the nonzero correlations between ions whose separations lie in the direction of near neighbors for a crystal held at a pressure of 6.7 GPa. (The correlation is zero whenever $\hat{\mathbf{x}}_j$ has no projection in the $\hat{\mathbf{x}}_i$-**S** plane.) Four results are plotted representing the sequential approximation from the real crystal to the analytically amenable idealization. The first three plotted results are numerically calculated, and the final result is analytical. The plots are for the actual crystal at 6.7 GPa, and the three successively imposed conditions: use of the small-momentum rather than the full form of the dynamical matrix, use of an isotropic set rather than the real set of elastic constants, and use of a sphere rather than the actual Brillouin zone. In imposing the last condition, the transition to the idealization is complete.

For demonstration of the extent of agreement between the four cases, separation distance between ions is treated as a continuous quantity. The first few actual site-separation distances are indicated with arrows.

VII. PRESSURE DEPENDENCE OF THE CORRELATION FUNCTION

The correlations are immediately associated with a length by taking their square root. In Figure 4 the dimensionless ratio of the correlation length to the nearest-neighbor dis-

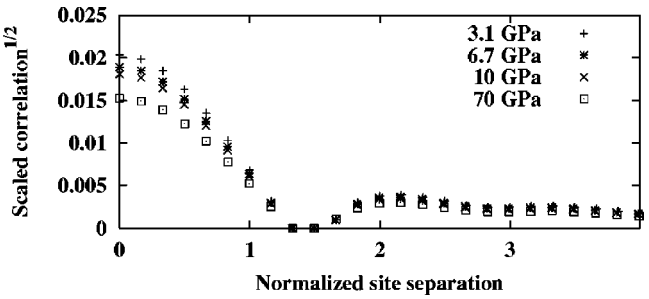

FIG. 4. The square root of the x-x correlation function plotted with ion separation along the (110) direction, both normalized to nearest-neighbor distance, for various pressures. The tics represent actual lattice sites.

tance is plotted with the dimensionless, normalized ion-ion separation along the (110) direction. The figure corresponds to the exact calculation, Eq. (3). Actual lattice sites are represented by the tics in the figure. The delocalization length associated with the autocorrelation decreases from 2% to 1.5% of the nearest-neighbor distance as the pressure is increased from 3.1 GPa to 70 GPa. This result, together with Van Hove's ansatz, suggests that ground-state anharmonic effects are less important at higher pressure. This conjecture is motivated by recognizing that the higher-order correlations—which are proportional to products of lower-order correlations—must diminish more quickly than the pair correlations. Therefore as the pair correlations decrease, the ions are less and less subject to the anharmonic forces associated with displacements appearing in the higher-order correlations. This is a familiar many-body result, where perturbations rise less rapidly than confinement energy as the density is increased.

VIII. CONCLUSIONS

Our study of the pressure dependence of the lattice dynamics and elastic properties of solid argon confirms earlier findings that the local-density approximation is problematic at low pressures, and improves at high pressures. We extend structural calculations to the ion correlation function. The analytical and exact results correspond as well as may be expected, and straightforward numerical approaches appear sufficient in spite of concerns about sensitivity to sampling near the Γ point. The impact of the small-momentum approximation is the largest among the three, and tends to suppress the autocorrelation function by $\approx 20\%$. At the same lattice vector, the correlations for varying displacement orientations are of the same order (where not zero by symmetry). While there is an order of magnitude decrease from the autocorrelation to that of the nearest neighbors, the dimensionless parameter associated with the correlation decays more slowly, from 2% for the on-site correlation to just under 1% for nearest ions at 6.7 GPa. Roughly similar behavior with increasing lattice vector is demonstrated at other pressures. The dimensionless correlation parameter associated with the autocorrelation is about 2% at 6.7 GPa, and falls to about 1.5% at 70 GPa. This suggests that the anharmonic nature of the crystal's ground state is suppressed at higher pressures.

[1] G. Placzek, B.R.A. Nijboer, and L. Van Hove, Phys. Rev. **82**, 392 (1951).
[2] M. Born, Rep. Prog. Phys. **9**, 294 (1943).
[3] M. Ferconi and M.P. Tosi, J. Phys.: Condens. Matter **3**, 9943 (1991).
[4] D. Pines, *Elementary Excitations in Solids* (Benjamin, New York, 1963).
[5] K. Lonsdale, Proc. R. Soc. London, Ser. A **179**, 8 (1942).
[6] V.Y. Naysh, Fiz. Met. Metalloved. **77**, 48 (1994).
[7] P. Rabe, G. Tokiehn, and A. Werner, J. Phys. C **12**, L545 (1979).
[8] A. Kirfel, J. Grybos, and V.E. Dmitrienko, Phys. Rev. B **66**, 165202 (2002).
[9] O.H. Nielsen and W. Weber, J. Phys. C **13**, 2449 (1980).
[10] A. Debernardi, S. Baroni, and E. Molinari, Phys. Rev. Lett. **75**, 1819 (1995).
[11] G. Lang, K. Karch, M. Schmitt, P. Pavone, A.P. Mayer, R.K. Wehner, and D. Strauch, Phys. Rev. B **59**, 6182 (1999).
[12] A. Debernardi, Solid State Commun. **113**, 1 (2000).
[13] M. Canonico, C. Poweleit, J. Menéndez, A. Debernardi, S.R. Johnson, and Y.H. Zhang, Phys. Rev. Lett. **88**, 215502 (2002).
[14] L. Van Hove, N.M. Hugenholtz, and L.P. Howland, *Quantum Theory of Many-Particle Systems* (Benjamin, New York, 1961).
[15] F. Occelli, M. Krisch, F. Sette, R. Le Toullec, C. Masciovecchio, and J.P. Rueff, J. Chem. Phys. **117**, 5859 (2002).
[16] H. Shimizu, H. Tashiro, T. Kume, and S. Sasaki, Phys. Rev. Lett. **86**, 4568 (2001).
[17] M. Grimsditch, P. Loubeyre, and A. Polian, Phys. Rev. B **33**, 7192 (1986)
[18] Y. Fujii, N.A. Lurie, R. Pynn, and G. Shirane, Phys. Rev. B **10**, 3647 (1974).
[19] T. Iitaka and T. Ebisuzaki, Phys. Rev. B **65**, 012103 (2001).
[20] T. Nakamura and H. Nagara, High Press. Res. **23**, 3 (2003).
[21] J. Tse, D. Klug, V. Shpakov, and J. Rodgers, Solid State Commun. **122**, 557 (2002).
[22] T. Tsuchiya and K. Kawamura, J. Chem. Phys. **117**, 5859 (2002).
[23] K. Rościszewski, B. Paulus, P. Fulde, and H. Stoll, Phys. Rev. B **62**, 5482 (2000).
[24] P. Hohenberg and W. Kohn, Phys. Rev. **136**, B864 (1964); W. Kohn and L.J. Sham, Phys. Rev. **140**, A1133 (1965); J. Perdew and A. Zunger, Phys. Rev. B **23**, 5048 (1981).
[25] D.R. Hamann, M. Schlüter, and C. Chiang, Phys. Rev. Lett. **43**, 1494 (1979).
[26] D. Vanderbilt, Phys. Rev. B **32**, 8412 (1985).
[27] L. Kleinman and D.M. Bylander, Phys. Rev. Lett. **48**, 1425 (1982).
[28] M.T. Yin and M.L. Cohen, Phys. Rev. B **26**, 3259 (1982).
[29] C. Kittel, *Introduction to Solid State Physics*, 3rd ed. (Wiley, New York, 1966).